RSC Advances

ROYAL SOCIETY OF CHEMISTRY

www.rsc.org/advances

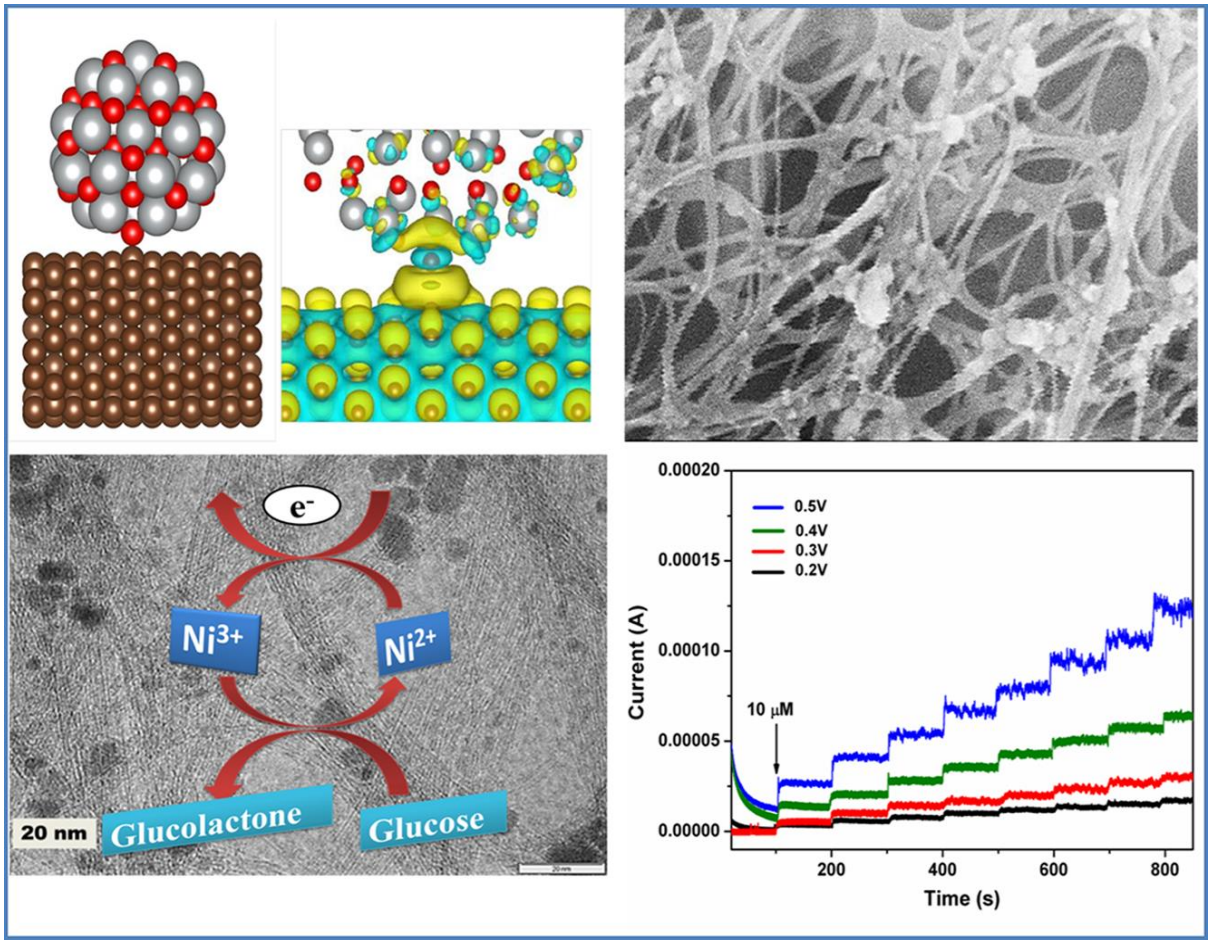

Plant root nodule like nickel-oxide / multi-walled carbon nanotube composites for non-enzymatic glucose sensor

Raghavendra Prasad[1], Narjes Gorjizadeh[2], Ravindra Rajarao[2], Veena Sahajwalla[2] and Badekai Ramachandra Bhat[1]*

[1]*Catalysis and Materials Laboratory, Department of Chemistry, National Institute of Technology Karnataka, Surathkal, Srinivasnagar-575025, India*

[2]*Centre for Sustainable Materials Research and Technology (SMaRT), School of Materials Science and Engineering, University of New South Wales, Sydney, NSW 2052, Australia*

* Corresponding author e-mail: ram@nitk.edu.in

Abstract

Herein, in this work we synthesized the plant root nodule like NiO-MWCNT nanocomposites by simple, rapid and solvent-free method using nickel formate as a precursor. Using first-principle simulation study the interactions and charge transfer behaviour of the NiO and MWCNT composite is investigated. The as-prepared NiO-MWCNT composite is employed to fabricate modified non-enzymatic carbon paste electrode (CPE) for glucose sensing. From the electrochemical investigation, fabricated sensor shows an excellent sensitivity of 6527 μA mM^{-1} cm^{-2} with the detection limit of 19 μM and linear response over a range from 0.001 mM to 14 mM of glucose concentration, at an applied potential of 0.5 V. Importantly sensor also exhibits greater stability, selectivity and reproducibility. First principle simulation study shows the differences in charge density and charge transfer behaviour from nanotube to NiO nanoparticle, which in turn enhances the electro catalytic property of NiO-MWCNT composite. Hence, these results indicate that NiO-MWCNT composite is a potential material for non-enzymatic electrochemical glucose sensor.

Keywords

Carbon nanotube; Composites; Glucose oxidation; Non-enzymatic sensor;

1. Introduction

The rapid and accurate determination of glucose has received significant attention due to its applications in various fields, such as clinical diagnostics, biotechnology and food industries.[1,2] Previous studies on this concern, largely focuses on glucose oxidase (GOx) based biosensor which catalyses the oxidation of glucose to glucolactone. This enzyme based biosensor, despite of possessing high selectivity and lower detection limit is associated with serious disadvantages like poor selectivity, complex enzyme immobilization procedures, high cost and instability to chemical toxicity, temperature, pH, humidity, limiting the wide range applications.[3-5] To overcome these limitations, direct oxidation of glucose using non-enzymatic biosensors have been explored in the recent decades.

Several electro-catalysts were reported on the direct electrochemical oxidation of glucose such as transition metals and metal-oxides (Au, Pt, Co, Cu, Ni, Co_3O_4, NiO, WO_3, RuO_2, etc.).[6-12] Among which NiO is relatively cheaper with high abundance, less toxicity and is suitable for several applications.[13] Fleischmann et al. 1971 reported that, Ni can serve as high potential electroctalyst for direct glucose oxidation resulting from the redox couple of $Ni^{3+/}Ni^{2+}$ in the basic medium.[14] Therefore there has been substantial investigation on Ni-based materials for the fabrication of non-enzymatic biosensors. Many non-enzymatic sensors have been fabricated using nickel based nanoparticles (NPs), nickel-carbon composites, nickel nanowires or porous nickel nanomaterials, etc.[15-20] However, these modified electrodes exhibit distinct features like high surface to volume ratio, enhanced electro-catalytic activity, as well as biocompatibility when compare with that of bulk electrodes.

In addition, Wang et al. in 2007 reported that the direct oxidation of carbohydrate and other organic compounds is greatly enhanced by the use of carbon nanotubes (CNTs)-metal hybrid modified electrode.[21] The CNTs are well known for their distinctive electrical and mechanical properties. However, composites of CNT with NiO shows improved properties like faster electron transfer kinetics, high surface area, least surface fouling, reduced overvoltage effects, excellent electro-catalytic activity, greater chemical and thermal stability than the individual CNT or NiO. Hence, composites of CNT are largely used in the fabrication of biosensors.[22-29] There are several methods reported to synthesize CNT-metal composites like wet impregnation, ball-milling, sputtering, electro-deposition, etc.[20, 30-33] However, bulk, simple and precise controlled nanoparticle decoration on CNT is still challenging and there are only few studies reported on bulk scale synthesis of NiO-MWCNT composite and its application as a non-enzymatic glucose sensor.

Hence, in this article, we report simple, rapid, solvent-free method for scalable synthesis of NiO-MWCNT composites and as-synthesized composites were characterised by field emission scanning electron microscopy (FESEM), transmission electron microscopy (TEM), X-ray diffraction (XRD) and Laser Raman spectroscopy (LRS). The first-principle calculations were used to investigate the interactions and charge transfer behaviour between MWCNT and NiO. The as-synthesized composites were used to construct the non-enzymatic glucose sensor and performance factors like sensitivity, selectivity, stability, linear range, limit of detection (LOD), interference effect and reproducibility are systematically investigated. For the best of our knowledge, to achieve the solvent-free method nickel formate was used as a precursor for the first time.

2. Experimental

2. 1 Reagents and solutions

D-Glucose, dopamine (DA), uric acid (UA), L-ascorbic acid (AA), glycine (Gly), tryptophan (Trp), nickel sulphate, sodium formate, graphite powder were procured from Sigma–Aldrich. All chemicals were used as received without any further purification. The MWCNTs were synthesized, purified and functionalised using the reported procedure from our research group.[34] Nickel formate was synthesized by refluxing nickel sulphate and sodium formate solution in stoichiometric amount and is confirmed by (powder) PXRD analysis (Fig. SI.1). The Human blood serum (HBS) samples were voluntarily given by the patients for conducting the experiments and study protocol was approved by the institutional review board at National institute of Technology Karnataka. Patients gave voluntary written informed consent before their participation.

2.2 Synthesis of NiO-MWCNT composites

Nickel formate was used as a precursor for the first time to achieve the solvent-free, rapid and scalable synthesis of NiO-MWCNT composite. The MWCNTs (0.25 g) was dry mixed with nickel formate (0.025 g) using mortar and pestle until the homogeneous mixture was obtained. The mixture was then transferred to quartz boat and subjected to thermal treatment in an air atmosphere at 380 °C for 2 h using chemical vapour deposition setup. The final product, NiO-NPs decorated MWCNTs were collected as a black powder and was used without further purification. For the comparison studies the pure NiO was synthesized similarly.

2.3 Electrode fabrication

The carbon paste electrode (CPE) was constructed by mixing graphite powder (0.7 g) and of silicone oil (0.3 g) in a mortar and pestle to produce a homogeneous paste which was then packed into the cavity of Teflon tube and electrical contact was established using a copper wire, which was then surface smoothened on a weighing paper. Similarly, the modified electrodes were fabricated using 0.05 g of NiO-MWCNT, pure NiO and MWCNT namely NiO-MWCNT/CPE, NiO/CPE and MWCNT/CPE respectively.

2.4. Theoretical simulation method

The calculations have been performed using first-principle plane-wave approach, based on the spin-polarized density-functional theory (DFT), in the generalized gradient approximation (GGA), with projector augmented-wave (PAW) pseudo-potentials, as implemented in Vienna Ab-initio Simulation Package (VASP).[35] The cut-off energy for the plane-wave expansion was set to be 400 eV. Structure including a NiO nanoparticle with diameter of 10Å on a (6,6) carbon nanotube with length of 14.7Å was embedded in a supercell with periodic boundary conditions. The supercell contains a vacuum of 10Å in the two direction perpendicular to nanotube axis in order to avoid interaction between neighbouring supercells. Using a 1x1x1 k-point mesh, the structures were optimized with force threshold of 0.05 eV/ Å.

3. Results and discussion

3.1 Theoretical simulation results

Geometry of the optimized structure is shown in Fig. 1(a). DFT calculations provide charge density of the optimized structure. To visualize the charge transfer between NiO and nanotube, we show in Fig. 1(b) the charge density difference in the geometrically optimized

system relative to isolated carbon nanotube and isolated NiO nanoparticle. The charge density difference plot shows redistribution of the charge in carbon nanotube upon adsorption of NiO nanoparticle. A significant charge accumulation is observed at the interface between the nanotube and the nanoparticle, and at the π orbitals of the carbons in the nanotube, while charge depletion appears mainly at sigma bonds of the nanotube. From the isosurface of charge density difference a charge transfer from nanotube to NiO nanoparticle can be observed.

3.2. Material characterization

The morphology of MWCNT and NiO/MWCNTs composite was examined by FESEM and their respective micrographs are as shown in Fig. (2a-c). An overview of the FESEM images shows that the pure MWCNT with length up to several micrometers and few nm of diameters, with no impurity on the surface of tube (Fig. 2a). However NiO decorated MWCNTs, appears to be randomly distributed with uneven nanoparticles decorated on the surface of the MWCNT tubes which resembles the plant root nodules (Fig. 2b and c). To investigate the further morphological features of the NiO-MWCNT composite TEM results were examined. From the TEM micrographs (Fig. 2d), it is observed that the dark stain on the MWCNT which attributes to the NiO-NPs wrap around the CNT with an average diameter of 15 to 20 nm. Fig. (3a) shows XRD pattern of the pure MWCNTs, NiO and NiO-MWCNT composites respectively. In the NiO-MWCNT composite samples the major peaks corresponding to MWCNTs and pure NiO were observed. The MWCNTs showed a typical (002) reflection at 26.3° and the NiO diffraction planes of (111), (200) and (220) reflections at 37.2°, 43.2° and 62.8°, can be distinctly indexed to the pure bunsenite form of NiO (JCPDS No. 74-2075). The broad diffraction peak for NiO in the composites signifies that, particles are nano-crystalline in nature.[36] Finally, there were no extra peaks observed from other crystal structures in the XRD spectrum indicating the high purity of the prepared

sample. Raman spectra were also recorded to study the defects in MWCNT before and after the composite synthesis as shown in Fig. (3b).The spectrum showed two typical peaks at 1344 and 1586 cm^{-1}, which may be assigned to D-band (disorder band) and G-band (graphite band), respectively. The G-band corresponds to the vibration of sp^2 bonded carbon atoms in a graphite layer with an E_{2g} mode of hexagonal graphite and the D-band is associated with vibration of carbon atoms with dangling bonds in the plane terminations of disordered graphite. The small broad peaks observed at the lower shift values are believed to arise from the formation of NiO.[37] Generally, the value of I_D/I_G ratio can be used to evaluate the disorder degree of the samples.[38, 39] In this case, obviously NiO-MWCNT showed larger I_D/I_G ratio (1.5) than MWCNT (0.6) indicating, more defects in composite sample and confirms the formation of NiO-MWCNT composite.

3.3. Electrochemical properties

The electrocatalytic activity of the as constructed modified electrodes towards glucose oxidation was investigated by cyclic voltammetry (CV) and chronoamperometry (CA). The cyclic voltammograms were recorded at the scan rate of 50 mV s^{-1} in the potential range from 0 to 0.8 V using 0.1 M NaOH solutions. The bare CPE shows no redox peaks and records least current, whereas, MWCNT/CPE did not show any redox peaks but records three folds higher current than the bare CPE which can be attributed to the high surface area and high electrical conductivity of MWCNT (Fig SI. 2). [28,40] However, the NiO/CPE shows the well-defined redox peaks in an alkaline solution which can be attributed to the redox couple of Ni that is Ni^{3+}/Ni^{2+} which cause for direct oxidation of glucose to glucolactone (Fig SI.2). [42, 18] The CVs of the modified electrodes namely, MWCNT/CPE, NiO/CPE and NiO-MWCNT/CPE in the absence and presence of glucose (curve a-e) are shown the Fig. (4a). There was no current response observed for MWCNT/CPE (curve a), whereas well-defined quasi-reversible redox peaks were observed for the NiO/CPE (curve b) and

NiO-MWCNT/CPE (curve d) with anodic peak potential at 0.516 V and the cathodic peak at 0.442 V, which attribute to the Ni^{3+}/Ni^{2+} redox couple. After the addition of the 1 mM glucose, increase in oxidation and reduction peak current density, indicates the NiO can electrocatalyze the direct oxidation of glucose in 0.1 M NaOH solution and similar results were reported on glucose detection using NiO-based materials.[41] Interestingly, the redox peak for NiO-MWCNT/CPE negative shifted anodic peak potential at 0.47 V and the cathodic peak at 0.33 V were observed and current density increases 2.5 folds (curve e) than the only NiO/CPE (curve c). The shifts in anodic peak potential to lower potential region may be due to the faster diffusion of glucose at the electrode surface and these results, indicates that NiO-NPs deposited on the MWCNT exhibits higher electrocatalytic activity toward the direct oxidation of glucose which is due to, MWCNTs providing large surface area and high conductivity for fast electron transfer improving the electron transduction.

The possible mechanism for oxidation of glucose by NiO-based materials could be represented by the following reactions.

$$NiO + OH^- \rightarrow Ni(OH)_2 \quad (1)$$

$$Ni(OH)_2 + OH^- \rightleftharpoons NiO(OH) + H_2O + e^- \quad \text{(or)}$$

$$Ni^{2+} + OH^- \rightarrow Ni^{3+} + e^- \quad (2)$$

$$NiO(OH) + glucose \rightarrow Ni(OH)_2 + Gluconic\ acid \quad \text{(or)}$$

$$Ni^{3+} + glucose \rightarrow Ni^{2+} + Gluconic\ acid \quad (3)$$

First, Ni^{2+} could be electro-oxidized to Ni^{3+} in 0.1 M NaOH solution where the release of electron resulted in the formation of oxidation peak current. Then, glucose ($C_6H_{12}O_6$) could be oxidized to gluconic acid ($C_6H_{12}O_7$) by Ni^{3+} which reduces to Ni^{2+} at the same time. Hence, the presence of glucose could lead to an increase in current. [18, 42, 43]

The effect of scan rate was studied for NiO-MWCNT/CPE as shown in the Fig. (4b), it is observed that for 1.0 mM glucose concentration in 0.1 M NaOH solution the redox peak current increased as the scan rate increasing from 10 mV to 500 mV. The redox peaks current were found to be linear to square root of scan rate with correlation coefficient of 0.9947 and 0.9938 respectively for anodic and cathodic current (inset Fig.4b).The obtained results demonstrate that the electrocatalytic glucose oxidation is a diffusion-controlled process and the peak to peak potential separation (ΔE_p) proportionally increases with the increase of the scan rate indicates charge-transfer kinetic limitations.[44-46]

For the further investigation of electrochemical properties of the NiO-MWCNT/CPE chronoamperometry response was recorded. Fig. 4c shows a typical current-time plot of the NiO-MWCNT/CPE electrode on successive additions of 10 μM of glucose. The constant stirring (350 rpm) was provided to achieve an instant homogeneous glucose concentration. With the step wise addition of glucose, the amperometric response also shows a step-like increase in current density. The amperometric response of NiO-MWCNT/CPE electrode were recorded at different applied potentials such as 0.2 V, 0.3 V, 0.4 V and 0.5 V respectively, are as shown in the Fig. 4c. A significant well defined, stable and rapid current change was observed with successive addition of 0.5 mM of glucose and achieving the steady state current in less than 3 s. The proposed sensor exhibit higher sensitivity in an applied potential of 0.5 V as compared with that of the 0.2 V, 0.3 V and 0.4 V which is supported from the CV results, where at ~ 0.47 V highest glucose oxidation peak current was observed and which is close to the 0.5 V hence, the 0.5 V is considered as optimised working potential. However, the higher noise is observed at 0.4 V which is due to intermediate species adsorbed onto the electrode surface with increased concentration and longer reaction time. At the different applied potential, amperometric current versus total glucose concentrations and the corresponding calibration curve are shown in Fig.4d. The sensitivity, detection limit,

response time and regression value were determined at different applied potential are tabulated in table 1. The sensor shows the highest sensitivity of 6527 μA mM^{-1} cm^{-2}, at 0.5 V with the detection limit of 19 μM which is greater than the other applied potential sensitivity of 3818.5 μA $mM^{-1}cm^{-2}$, 1552 μA $mM^{-1}cm^{-2}$, 931 μA $mM^{-1}cm^{-2}$ at an applied potential of 0.4 V, 0.3 V and 0.2 V respectively. From these obtained results, it is observed that sensor shows the greater electrocatalytic activity at an applied potential of 0.5 V. Hence the further interference and stability studies were performed at applied potential of 0.5 V.

To investigate the interference effect of DA, UA, Gly, AA and Trp towards the determination of glucose, which commonly co-exist with glucose in real samples (human blood). The effect of interference was studied by recording the amperometric response for the above said molecules of concentration 0.2 mM at the applied potential of 0.5 V is shown in Fig. 5a. There is no distinct current response observed with the addition of 0.2 mM DA, UA, Gly, AA and Trp. On the contrary, a significant current response with the addition of 0.2 mM glucose appeared. Hence, the current response of common interfering biomolecules caused negligible interference to the response of glucose at NiO-MWCNT/CPE. The long term stability of the sensor was evaluated by measuring amperometric current responses to 0.2 mM L^{-1} glucose for 30 days period (Fig. 5b). The results show that the NiO-MWCNT/CPE retained 90% of its initial current response to glucose which could be mainly ascribed to the chemical stability of NiO/MWCNTs where in which I is the current response at first day and I_0 is the current recorded at subsequent days. The proposed sensor was compared for its sensitivity, limit of detection and for its linear range with the previously reported work are as shown in table 2. However, the sensor show high sensitivity of 6527 μA mM^{-1} cm^{-2} which is much higher than any other CNT based non-enzymatic sensor reported previously. [4,3, 47-50] Hence, these results demonstrate that NiO-MWCNT composite is a promising material for the fabrication of the non-enzymatic glucose sensor.

Finally, as a real application, the NiO-MWCNT/CPE was applied to the determination glucose concentration in human blood serum samples (HBS). HBS without any pre-treatment was injected into 5 mL of 0.1 M NaOH at an applied potential of +0.5 V. The measured current change was correlated with the glucose concentration according to the calibration curve in Fig. SI.3 and then compared with the value obtained using a commercial glucose meter (Free Style Freedom Lite Glucose Monitoring System, Abbott Diabetes Care) as shown in the table 3. The results show that recovery of the samples are > 95 % with the relative standard deviation (RSD) less than 5 %. Hence, these results suggest that, the proposed NiO/MWCNT composite, a potential material for the fabrication of enzyme-free glucose sensors.

4. Conclusions

Using simple, solvent-free method, plant root nodule like NiO-MWCNTs nanocomposites were successfully synthesized and used to fabricate the non-enzymatic electrochemical sensor for glucose detection. Under the optimal conditions, as-fabricated non-enzymatic sensor shows the excellent sensitivity of 6527 μA mM^{-1} cm^{-2} at an applied potential of +0.5 V and a detection limit of 19 μM was achieved. Because of the ease of composite synthesis and the excellent electrochemical sensing properties, the NiO-MWCNT are expected to serve as a promising material for the development of the non-enzymatic glucose sensor.

Acknowledgements

The authors are grateful to Intersect Australia Ltd. Australia, for Computational resources, Centre for Science and Engineering (CeNSE), Bangalore for providing analytical facilities and National Institute of Technology Karnataka, Surathkal for the research fellowship.

References

1. S. Fu, G. Fan, L. Yang and F. Li, Electrochim. Acta, 2015, 152, 146-154.
2. T. Choi, S. H. Kim, C. W. Lee, H. Kim, S.-K. Choi, S.H. Kim, E. Kim, J. Park and H. Kim, Biosens. Bioelectron., 2015, 63, 325-330.
3. S. Park, H. Boo and T. D. Chung, Anal. Chim. Acta, 2006, 556, 46-57.
4. X. Kang, Z. Mai, X. Zou, P. Cai and J. Mo, Anal. Biochem., 2007, 363, 143-150.
5. X. Li, Q. Zhu, S. Tong, W. Wang and W. Song, Sens. Actuators, B, 2009, 136, 444-450.
6. W. Wang, L. Zhang, S. Tong, X. Li and W. Song, Biosens. Bioelectron., 2009, 25, 708-714.
7. P. Si, Y. Huang, T. Wang and J. Ma, R. Soc. Chem. Adv. 2013, 3, 3487-3502.
8. C. Guo, H. Huo, X. Han, C. Xu and H. Li, Anal. Chem., 2013, 86, 876-883.
9. C. Guo, Y. Wang, Y. Zhao and C. Xu, Anal. Methods, 2013, 5, 1644-1647.
10. G. Wang, X. He, L. Wang, A. Gu, Y. Huang, B. Fang, B. Geng and X. Zhang, Microchim. Acta, 2013, 180, 161-186.
11. C. Guo, X. Zhang, H. Huo, C. Xu and X. Han, Analyst, 2013, 138, 6727-6731.
12. H. Huo, C. Guo, G. Li, X. Han and C. Xu, R. Soc. Chem. Adv., 2014, 4, 20459-20465.
13. J. Li, F. Meng, S. Suri, W. Ding, F. Huang and N. Wu, Chem. Commun., 2012, 48, 8213-8215.
14. M. Fleischmann, K. Korinek and D. Pletcher, J. Electroanal. Chem. Interfacial Electrochem., 1971, 31, 39-49.
15. L.M. Lu, L. Zhang, F.L. Qu, H.X. Lu, X.B. Zhang, Z.S. Wu, S.Y. Huan, Q.A. Wang, G.L. Shen and R.Q. Yu, Biosens. Bioelectron., 2009, 25, 218-223.
16. X. Xiao, J. R. Michael, T. Beechem, A. McDonald, M. Rodriguez, M. T. Brumbach, T. N. Lambert, C. M. Washburn, J. Wang, S. M. Brozik, D. R. Wheeler, D. B. Burckel and R. Polsky, J. Mater. Chem., 2012, 22, 23749-23754.
17. B. Wang, S. Li, J. Liu and M. Yu, Mater. Res. Bull., 2014, 49, 521-524.

18. G. Wang, X. Lu, T. Zhai, Y. Ling, H. Wang, Y. Tong and Y. Li, Nanoscale, 2012, 4, 3123-3127.

19. J. Wang, W. Bao and L. Zhang, Anal. Methods, 2012, 4, 4009-4013.

20. W.D. Zhang, J. Chen, L.C. Jiang, Y.X. Yu and J.Q. Zhang, Microchim Acta, 2010, 168, 259-265.

21. J. Wang, T. Tangkuaram, S. Loyprasert, T. Vazquez-Alvarez, W. Veerasai, P. Kanatharana and P. Thavarungkul, Anal. Chim. Acta, 2007, 581, 1-6.

22. J.S. Ye, Y. Wen, W. De Zhang, L. Ming Gan, G. Q. Xu and F.-S. Sheu, Electrochem. Commun., 2004, 6, 66-70.

23. V. G. Gavalas, S. A. Law, J. Christopher Ball, R. Andrews and L. G. Bachas, Anal. Biochem., 2004, 329, 247-252.

24. A. Merkoci, M. Pumera, X. Llopis, B. Pérez, M. del Valle and S. Alegret, TrAC Trends in Anal. Chem., 2005, 24, 826-838.

25. J. Wang and Y. Lin, TrAC Trends in Anal. Chem., 2008, 27, 619-626.

26. C. B. Jacobs, M. J. Peairs and B. J. Venton, Anal. Chim. Acta, 2010, 662, 105-127.

27. H.W. Chang, Y.C. Tsai, C.W. Cheng, C.Y. Lin and P.H. Wu, Sens. Actuators, B, 2013, 183, 34-39.

28. J. Zhao, L. Wei, C. Peng, Y. Su, Z. Yang, L. Zhang, H. Wei and Y. Zhang, Biosens. Bioelectron., 2013, 47, 86-91.

29. W.S. Kim, G.J. Lee, J.H. Ryu, K. Park and H.K. Park, R. Soc. Chem. Adv. 2014, 4, 48310-48316.

30. C.T. Hsieh, Y.W. Chou and W.Y. Chen, J Solid State Electrochem, 2008, 12, 663-669.

31. A. Sun, J. Zheng and Q. Sheng, Electrochim. Acta, 2012, 65, 64-69.

32. Z. G. Zhu, L. Garcia-Gancedo, C. Chen, X. R. Zhu, H. Q. Xie, A. J. Flewitt and W. I. Milne, Sens. Actuators, B, 2013, 178, 586-592.

33. S.u. Rather and K. S. Nahm, Mater. Res. Bull., 2014, 49, 525-530.

34. R. Rajarao and B. R. Bhat, Synthesis and Reactivity in Inorganic, Syn. React. Inorg. Met. Chem., 2013, 43, 1418-1422.

35. G. Kresse and J. Hafner, Phys. Rev. B, 1993, 47, 558-561.

36. J. Mun, H.W. Ha and W. Choi, J. Power Sources, 2014, 251, 386-392.

37. Y. Bai, M. Du, J. Chang, J. Sun and L. Gao, J. Mater. Chem. A, 2014, 2, 3834-3840.

38. U. J. Kim, C. A. Furtado, X. Liu, G. Chen and P. C. Eklund, J. Am. Chem. Soc., 2005, 127, 15437-15445.

39. G. E. Ioannatos and X. E. Verykios, Int. J. Hydrogen Energy, 2010, 35, 622-628.

40. H.X. Wu, W.M. Cao, Y. Li, G. Liu, Y. Wen, H. F. Yang and S.P. Yang, Electrochimica Acta, 2010, 55, 3734-3740.

41. M. A. Kiani, M. A. Tehrani and H. Sayahi, Anal. Chim. Acta, 2014, 839, 26-33.

42. C. Zhao, C. Shao, M. Li and K. Jiao, Talanta, 2007, 71, 1769-1773.

43. X. Li, A. Hu, J. Jiang, R. Ding, J. Liu and X. Huang, Journal of Solid State Chemistry, 2011, 184, 2738-2743.

44. Y. Mu, D. Jia, Y. He, Y. Miao and H.L. Wu, Biosens. Bioelectron., 2011, 26, 2948-2952.

45. J. Nai, S. Wang, Y. Bai and L. Guo, Small, 2013, 9, 3147-3152.

46. B. Rafiee and A. R. Fakhari, Biosens. Bioelectron., 2013, 46, 130-135.

47. H.F. Cui, J.S. Ye, W.D. Zhang, C.M. Li, J. H. T. Luong and F.S. Sheu, Anal. Chim. Acta, 2007, 594, 175-183.

48. J. Chen, W.D. Zhang and J.-S. Ye, Electrochem. Commun., 2008, 10, 1268-1271.

49. K.J. Chen, C.F. Lee, J. Rick, S.H. Wang, C.C. Liu and B.J. Hwang, Biosens. Bioelectron., 2012, 33, 75-81.

50. L.M. Lu, X. B. Zhang, G.L. Shen and R.Q. Yu, Anal. Chim. Acta, 2012, 715, 99-104.

51. K. Momma, F. Izumi, J. Appl. Crystallogr., 2008, 44, 1272–1276.

Table 1

Analytical performance of the proposed NiO-MWCNT/CPE electrode.

Sl.No	Applied potential (V)	Sensitivity ($\mu A\ mM^{-1}cm^{-2}$)	LOD (μM)	Response time (s)	Regression value (R^2)
1	0.2	931.4	38	3	0.9866
2	0.3	1552	58	2	0.9707
3	0.4	3818.5	24.5	4	0.9946
4	0.5	6527	19	2	0.9952

Table 2

Comparison of analytical performance of proposed NiO-MWCNT/CPE electrode with reported MWCNT based non-enzymatic glucose sensors.

Type of electrode	**Linear range (mM)**	**Detection limit (µM)**	**Detection potential**	**Sensitivity ($\mu A\ mM^{-1}\ cm^{-2}$)**	**Reference**
NiO/MWCNTs/ Ta substrate	Up to 7.0	2.0	0.50	1.77	[20]
CS-GA-GOx-Nafion-PtPd–MWCNT	0.062–14	31	0.60	112	[49]
Ni-multi-wall CNT	0.0032–17.5	0.89	0.60	67.2	[31]
MnO_2/MWNTs	Up to 28	N.A.	0.30	33.19	[48]
Pt–Pb/CNTs	Up to 0.5	1.8	0.30	~18	[47]
Cu nanocluster/ MWCNT	0.7–3.5	0.21	0.65	17.76	[4]
Cu/Au/CNT	0.0001–0.5	0.3	0.65	NA	[50]
NiO-MWCNT/CPE	0.001-0.5	38	0.2	931.4	Present work
NiO-MWCNT/CPE	0.001-0.5	58	0.3	1552	Present work
NiO-MWCNT/CPE	0.001-0.5	24.5	0.4	3818.5	Present work
NiO-MWCNT/CPE	0.001-14	19	0.5	6527	Present work

Table 3

The detection of glucose in human blood serum samples (HBS).

Sample	**Glucose (mM) (Proposed sensor)**	**RSD*** **(*N* = 4)**	**Glucose (mM) (commercial glucose sensor)**	**Recovery (%)**
1	5.8	4.5 %	5.6	98
2	4.5	4.2 %	4.32	96
3	7.0	3.7 %	6.74	96.4
4	3.8	3.5 %	3.75	98.7
5	6.7	4.6 %	6.55	97.8

*Average of four trials.

Figures

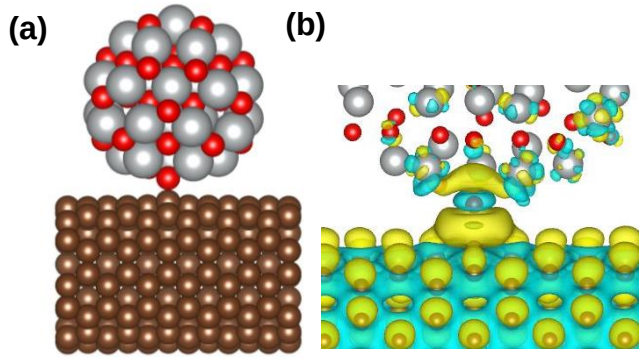

Fig. 1.(**a**) Geometrical position of the optimized structure of NiO nanoparticle on (6,6) carbon nanotube. (**b**) Charge density difference isosurface of NiO adsorbed on nanotube. Charge density difference gives the information about redistribution of charge in the system relative to isolated carbon nanotube and isolated NiO nanoparticle. Yellow and blue indicate charge accumulated region and charge depleted regions, respectively. The isosurface value is $3x10^{-3}$ e/Å^3. (Color scheme: C= brown, Ni= grey, O=red). The figure was drawn using Vesta software.[51]

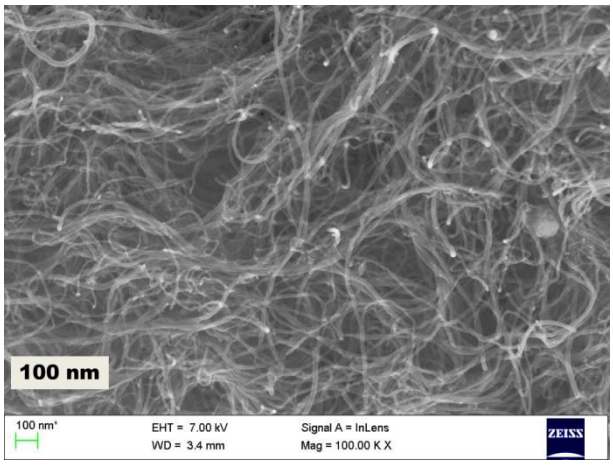

(a)

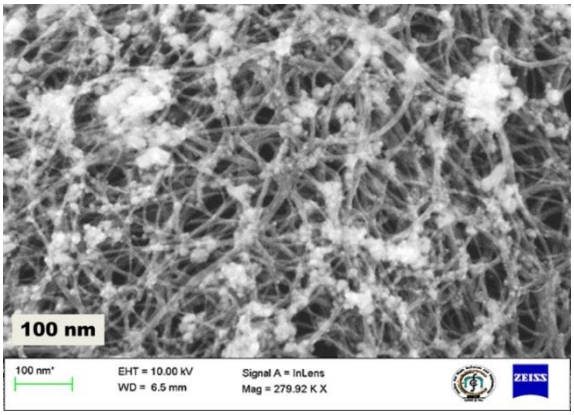

(b)

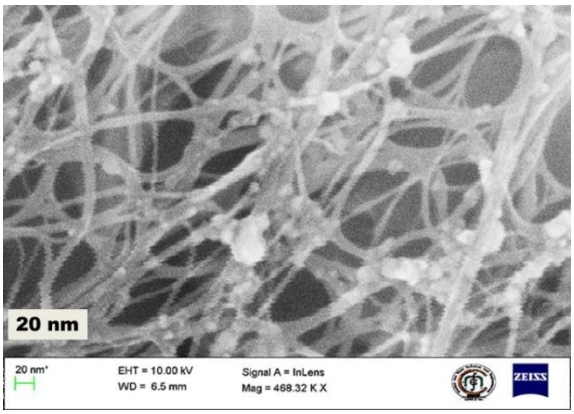

(c)

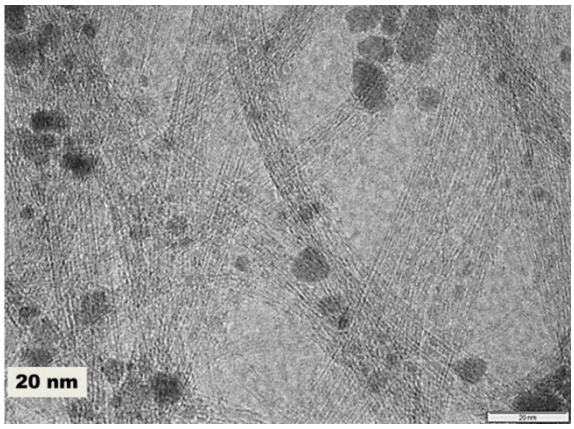

(d)

Fig. 2.FESEM images of **(a)** pure MWCNT **(b-c)** NiO-MWCNT composite **(d)** TEM image of NiO-MWCNT composite

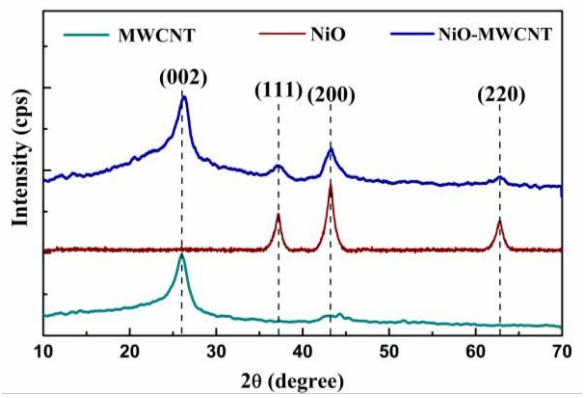

(a)

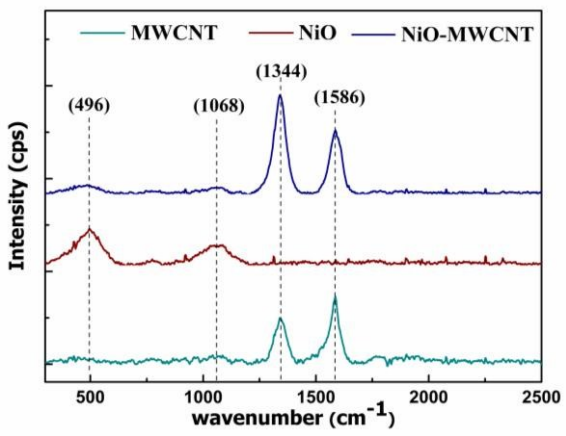

(b)

Fig. 3. (a) PXRD and (b) Raman spectra of NiO-MWCNT pure MWCNT in comparison with the pure NiO and NiO-MWCNT composite samples

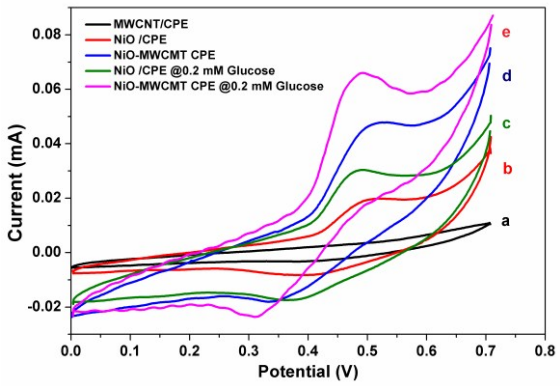

(a)

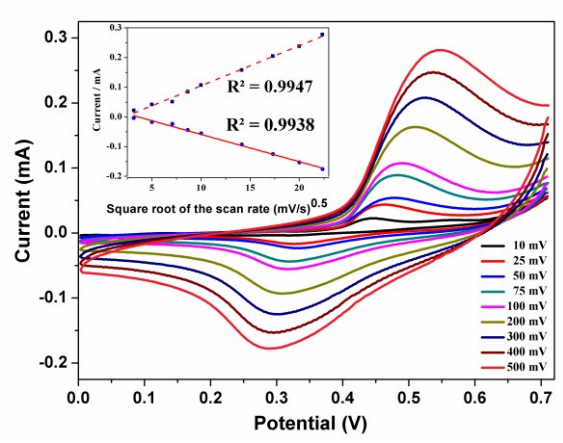

(b)

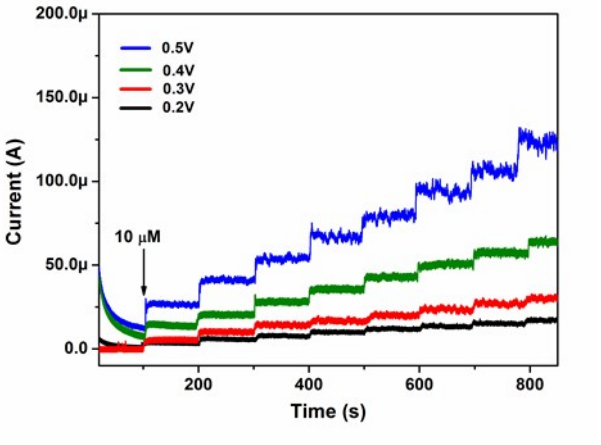

(c)

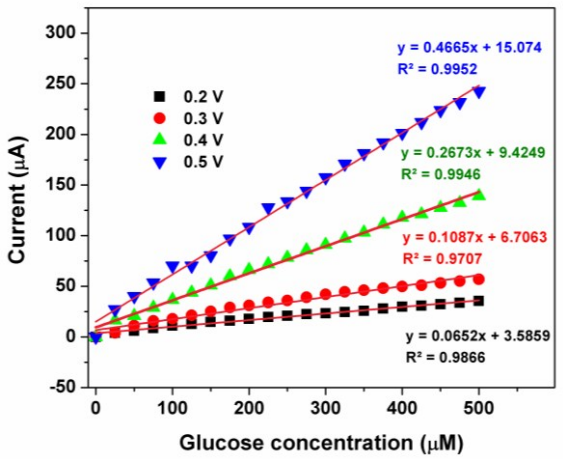

(d)

Fig.4. (a) CVs of different electrodes in the absence and presence of glucose, **(b)**CVs of NiO-MWCNT/CPE electrode at different scan rates from 10 to 500 mV s^{-1} in 0.1 M NaOH with 0.1 mM glucose (inset Fig. plot of peak current (I_P)vs. square root of scan rate ($\sqrt{\nu}$). (c) amperometric responses of NiO-MWCNT/CPE electrode upon the successive addition of 10 μM glucose (d) the amperometric current plotted vs. total glucose concentration, and their corresponding linear calibration curves.

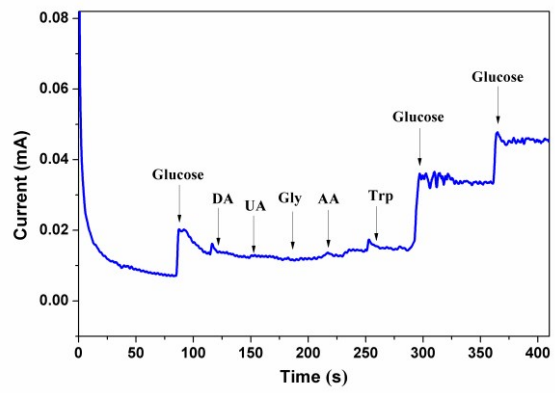

(a)

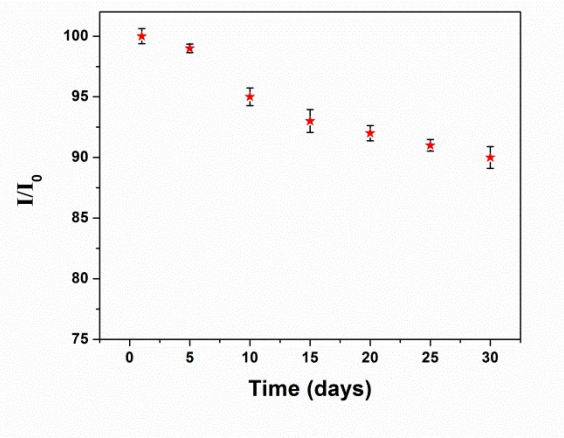

(b)

Fig.5. Chronoamperometric response of the NiO-MWCNT/CPE electrode on successive addition of 0.2 mM of glucose, DA, UA, UA, Gly, AA and Trp into 0.1 M NaOH solution.

(b) Stability plot for NiO-CNT/CPE sensor stored over three weeks in 0.1 M NaOH with 0.2 mM glucose at 0.5 V.